Physics of the Earth and Planetary Interiors 306 (2020) 106539

Contents lists available at ScienceDirect

Physics of the Earth and Planetary Interiors

journal homepage: www.elsevier.com/locate/pepi

Crustal modifications beneath the central Sunda plate associated with the Indo-Australian subduction and the evolution of the South China Sea

Jia Gao[a], Youqiang Yu[a,*], Wenkai Song[a], Stephen S. Gao[b], Kelly H. Liu[b]

[a] State Key Laboratory of Marine Geology, Tongji University, Shanghai 200092, China
[b] Geology and Geophysics Program, Missouri University of Science and Technology, Rolla, MO 65409, USA

ARTICLE INFO

Keywords:
Sunda plate
Sumatra Subduction
South China Sea
Crustal modification
Receiver function

ABSTRACT

To decipher possible crustal modifications associated with complex tectonics in SE Asia, we have conducted a systematic receiver function investigation beneath the central Sunda plate mainly including Borneo, the Malay Peninsula, Sumatra and part of the South China Sea (SCS). Well-determined observations from a total of 22 stations reveal a laterally heterogeneous crust with thickness ranging from 22.8 km to 39.1 km and Vp/Vs values varying from 1.68 to 2.12. An increasing pattern of Vp/Vs ratios towards the Sumatra fault and the Toba Caldera indicates significant modifications of crustal composition possibly due to melting from the Indo-Australian subduction. Crustal compositions beneath the Malay Peninsula are determined to be mostly felsic to intermediate rocks. Crustal thinning at the Sibumasu terrane relative to the East Malay block is revealed and may be attributed to joint effects of Late Paleogene rifting and a subsequent thermal anomaly. The southwards subduction of the hypothetical Proto-SCS may have contributed to the revealed magma intrusion and thinned crust beneath NW Borneo, and developed an accretionary setting at NE Borneo. The cessation of the Proto-SCS subduction further promotes collision between NE Borneo and Nansha block, which is supported by the observed crustal thickening. Thinned crust at the southern margin of the SCS basin is further confirmed as continental in origin and has been altered by possible post-spreading volcanisms.

1. Introduction

The Sunda plate of Southeast Asia is surrounded by the Indian plate to the west, Australian plate to the southwest and south, Philippine plate to the east, Yangtze plate to the northeast, and Eurasian plate to the north (Fig. 1). A large portion of the Sunda plate is composed of continental segments derived from Gondwana from Devonian to late Cretaceous (Metcalfe, 2002, 2011) and assembled during the Triassic Indosinian orogeny (Hall and Morley, 2004). The western edge of the Sunda plate is characterized by several strike-slip faults, including the Wang Chao and Three Pagodas fault systems, which accommodate the extrusion of the Indochina Peninsula as the result of India-Asia collision in the Cenozoic (Hall, 2002; Tapponnier et al., 1982). A series of marginal seas have developed in the Cenozoic on the eastern part of the Sunda plate, including the South China Sea (SCS) whose origin remains controversial (Hall, 2002).

Geographically, the study area (Fig. 1) is approximately situated at the central Sunda plate and comprises the Malay Peninsula, the southwestern SCS, the southern portion of the Indochina Peninsula, and the Sumatra and Borneo Islands. The Malay Peninsula was assembled in the late Triassic and is divided into the Sibumasu terrane and the East Malay Block by the Bentong-Raub Suture. The plutonic rocks in the Malay Peninsula are mostly (~90%) granitic while the western and eastern Malaya plutons are characterized as S-Type and I-Type granitoids, respectively (Metcalfe, 2013). Sumatra is underlain by continental crust dating from the Permo-Carboniferous and featured by the 1900-km-long dextral Sumatran fault and active volcanoes such as the Toba caldera associated with the subduction of the Indo-Australian plate (Fitch, 1972; McCaffrey, 2009). The volcanic chain with active andesitic volcanism is parallel to the subduction zone and situated along the Barisan Mountain Range (Sieh and Natawidjaja, 2000). The SCS developed on the South China continental margin between the early Oligocene and the middle Miocene (Briais et al., 1993; Hall, 2002; Taylor and Hayes, 1983). The development of the present SCS is believed to be partially or dominantly driven by the southward dragging from the Proto-SCS subduction beneath north Borneo (Hall, 1996; Hall et al., 2008), which promotes developing a non-volcanic accretionary setting. From Early-Middle Miocene, the Nansha block, which was separated from the South China margin due to the spreading of the SCS, underthrust north Borneo, a process that further induced uplift and

* Corresponding author.
E-mail address: yuyouqiang@tongji.edu.cn (Y. Yu).

https://doi.org/10.1016/j.pepi.2020.106539
Received 26 April 2020; Received in revised form 8 June 2020; Accepted 8 June 2020
Available online 09 June 2020

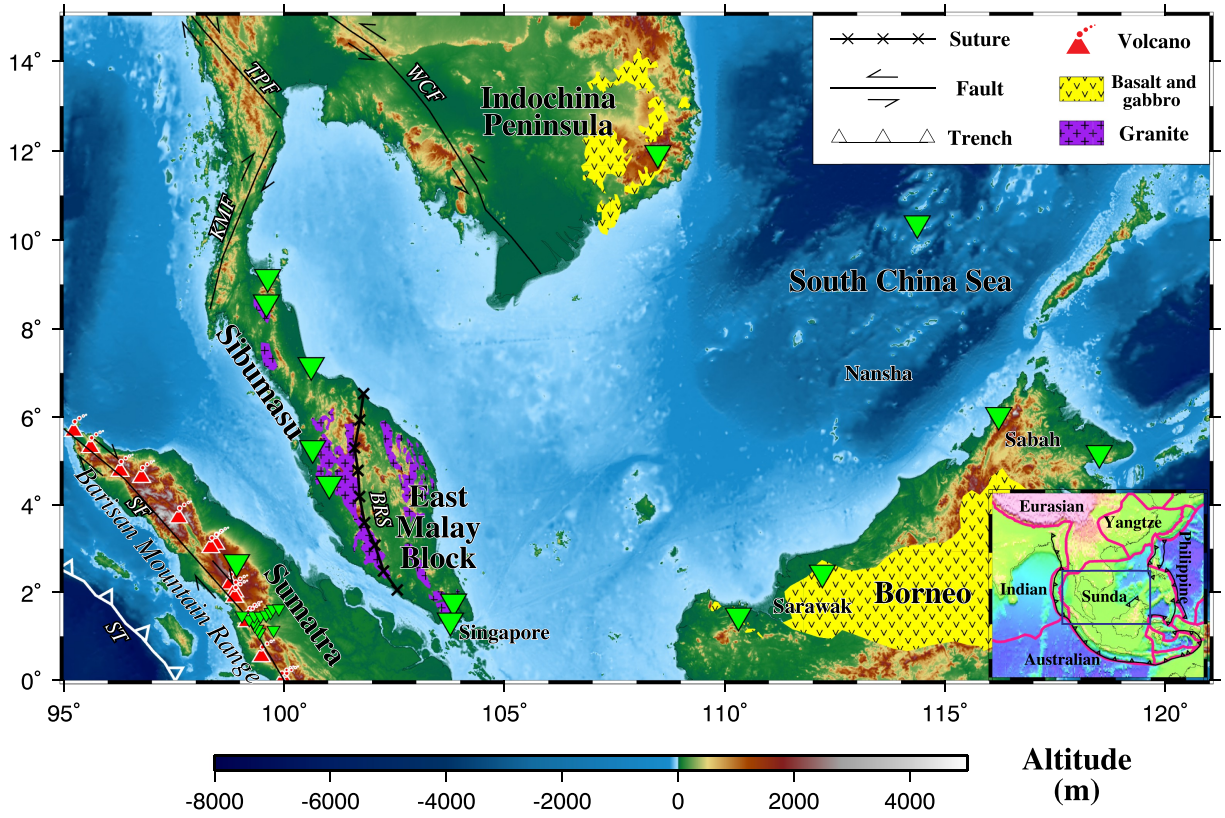

Fig. 1. Topographic map of the study area showing major tectonic features and the locations of seismic stations (green triangles). The distributions of the granite (Metcalfe, 2013; Searle et al., 2012), basalt and gabbro (Hoang and Flower, 1998; Hutchison, 1996) are depicted as purple and yellow shaded areas, respectively. Black lines denote major faults and sutures modified from Hall et al. (2008) and Metcalfe (2013): BRS (Bentong-Raub Suture), KMF (Khlong Marui Fault), SF (Sumatra Fault), TPF (Three Pagodas Fault) and WCF (Wang Chao Fault). The insert displays the location of the study area highlighted by the blue rectangle. The black line represents the trench, and the red lines are plate boundaries (Bird, 2003). (For interpretation of the references to colour in this figure legend, the reader is referred to the web version of this article.)

crustal thickening (Hall, 2002; Hall et al., 2008). Several other models (Sun, 2016) are also proposed for the development of the SCS such as those involving the extrusion of the Indochina Peninsula (e.g., Briais et al., 1993; Tapponnier et al., 1982) and mantle upwelling (e.g., Flower et al., 1998).

The central Sunda plate has been described as a stable shield or craton during most of the Cenozoic (e.g., Replumaz et al., 2004; Replumaz and Tapponnier, 2003) and rotated clockwise as a rigid block during the last 8–10 Ma (Rangin et al., 1999). Such a perception has been challenged by the observed low velocity anomalies in the lithosphere, high heat flow, and significant internal deformations (Hall, 1996; Hall and Morley, 2004), which may have left their imprints on the crustal structure and can be possibly deciphered by geophysical investigations. Based on seismograms recorded by a seismic array of the Toba Seismic Experiment, a magma reservoir is confirmed under the Toba caldera, beneath which the crustal thickness is found to be between 29 and 40 km (Sakaguchi et al., 2006). Crustal thickness determined from five stations belonging to Singapore's seismic network was revealed to vary from ~24 to ~32 km with a pronounced northeastward thinning (Macpherson et al., 2013). Broadband data from a total of 8 stations in the Malay Peninsula are recently employed to determine the crustal structure by joint inversion of surface wave dispersion and receiver function (RF). The Moho depth decreases northwards, from 34 km in the south to 26 km in the north, with V_P/V_S ratios mostly below 1.83 (Latiff and Khalil, 2019). Understanding of the crustal structure beneath the southern margin of the SCS is mostly from analysis of gravity and active-source seismic data (e.g., Qiu et al., 2011; Chang et al., 2017; Yu et al., 2017c). Volcanic basement structures associated with a high velocity or density lower crust is proposed to exist offshore north of Taiping Island in the Spratly (Nansha) islands area (Chang et al., 2017), which are contrary to the results from an earlier seismic study around the same area that suggests the absence of a high velocity lower-crustal layer (Qiu et al., 2011). Seismic reflection studies indicate that the Moho is much deeper beneath the southern continental margin of the SCS with an average value of about 22 km relative to its northern continental margin, where the Moho depth is about 18 km (Yu et al., 2017c). Previous crustal investigations largely focused on localized areas, and a comprehensive investigation on the crustal structure and its geodynamic implications beneath the central Sunda plate as a whole is still lacking.

In this study, we have employed all the broadband seismic data recorded by a total of 29 stations to conduct a systematic investigation of crustal structure beneath the central Sunda plate based on the RF method. A frequency-domain deconvolution technique is utilized to reduce strong reverberations on the RFs associated with an overlying low-velocity layer to more accurately constrain the resulting crustal thickness and V_P/V_S (Yu et al., 2015). Our observations provide additional constraints on crustal structure over a broader region than previous studies (e.g., Kieling et al., 2011; Latiff and Khalil, 2019; Macpherson et al., 2013) and shed new lights on crustal modifications associated with magmatic activities from different tectonic domains.

2. Data and methods

Broadband seismic data used in the study are publicly available and requested from the Incorporated Research Institutions for Seismology (IRIS) Data Management Center (DMC). The data set was recorded by 29 stations (Fig. 1) belonging to 7 seismic networks: Singapore

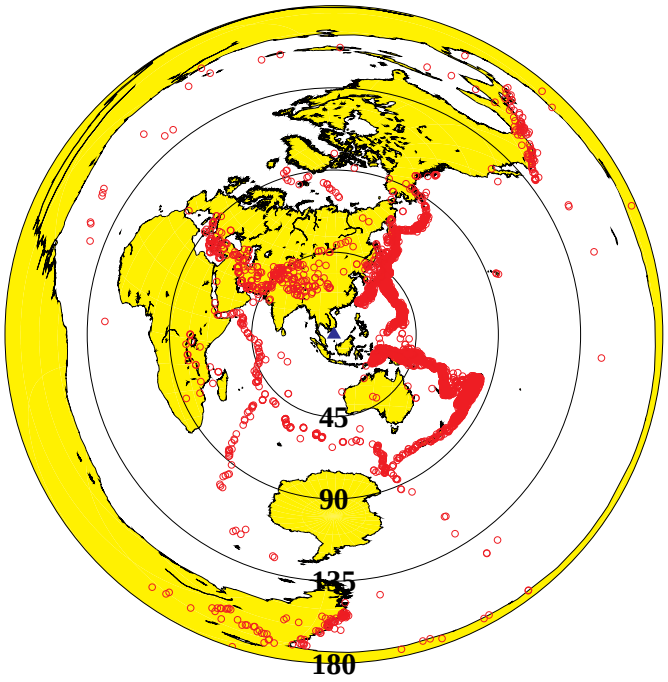

Fig. 2. Azimuthal equidistant projection map displaying the distribution of events (red circles) used in the study. The blue triangle represents the center of the study area. (For interpretation of the references to colour in this figure legend, the reader is referred to the web version of this article.)

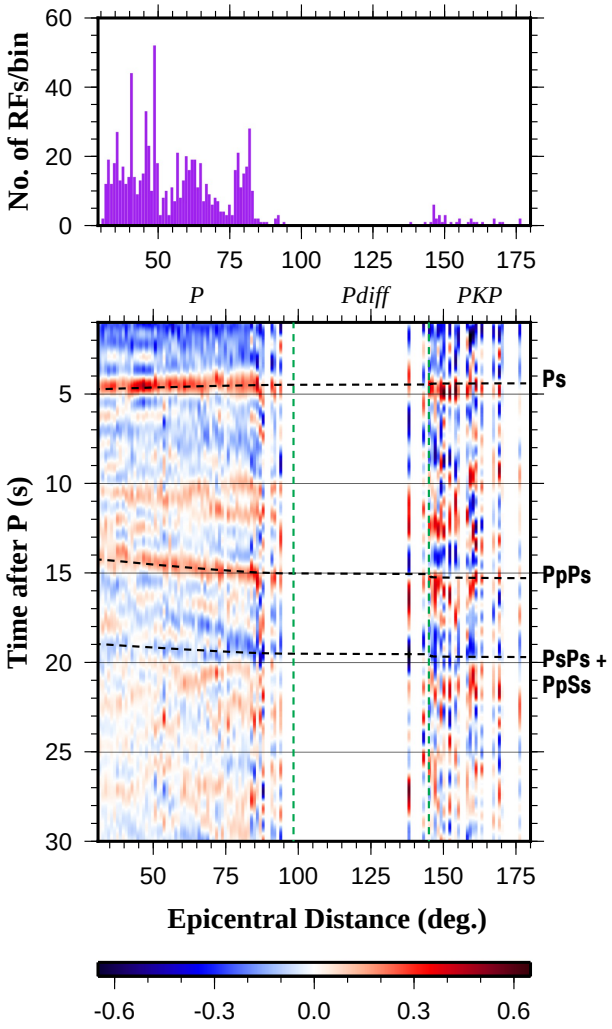

Fig. 3. (bottom) RFs recorded by station DLV stacked in epicentral distance bins and (top) the corresponding number of RFs. The RFs are grouped into epicentral distance bins of 1° and the amplitude is displayed relative to that of the first arrival. Horizontal dashed lines indicate the predicted arrival times of Ps, PpPs and PsPs + PpSs. Vertical dashed green lines divide the ranges of epicentral distance for P, Pdiff and PKP. (For interpretation of the references to colour in this figure legend, the reader is referred to the web version of this article.)

Seismological Network (MS), Malaysian National Seismic Network (MY), Pacific21 (PS), Regional Integrated Multi-Hazard Early Warning System (RM), Thai Seismic Monitoring Network (TM), Broadband Array in Taiwan for Seismology (TW), and Sumatra Segmentation and Aftershocks Deployment (ZB). Events were initially selected based on the following two criteria: (1) the epicentral distance is 30°–180° (Fig. 2) with the first arrivals including P, Pdiff and PKP (Fig. 3), and (2) the magnitude is equal to or greater than the cut-off magnitude (Mc) which is defined as $Mc = 5.2 + (\Delta - \Delta_{min})/(180.0 - \Delta_{min}) - D/700.0$, where Δ is the epicentral distance in degrees, $\Delta_{min} = 30°$, and D is the focal depth in kilometers (Liu and Gao, 2010). A total of 4835 events occurred over the period of 1993–2019 satisfy these criteria (Fig. 2). All the three component seismograms were windowed to 20 s before and 260 s after the first compressional-wave arrival calculated from the IASP91 Earth model, and then filtered by a 4 pole, 2 pass Butterworth band-pass filter with corner frequencies of 0.08 and 0.8 Hz. We followed the water level deconvolution procedure of Ammon (1991) to generate the radial RFs for those filtered seismograms with signal-to-noise ratio of 4.0 or greater on the radial component. The resulting RFs were further visually verified to make sure that only RFs with well-defined first compressional-wave arrivals were kept.

We employed the $H - k$ stacking method (Zhu and Kanamori, 2000) for moveout correction and stacking. The optimal crustal thickness (H) and V_P/V_S ratio (k) were determined by the maximum stacking amplitude on the $H - k$ plot (Fig. 4) obtained from a series of combinations of candidate H (in the initial range of 15–55 km with an interval of 0.1 km) and k (1.65 to 1.95 with a step of 0.01) values. $H - k$ plots for all the stations can be found in the supplementary file (Figs. S1–S6). The weighting factors used for the stacking were assigned as 0.5, 0.4 and 0.1 for the P-to-S converted phase (Ps) and its multiples (PpPs and PsPs + PpSs) from the Moho, respectively (Fig. 3). There were no significant changes of the results when different weighting factors were tested. After considering previous studies, a mean crustal P-wave velocity (Vp) of 6.1 km/s was chosen in the study, which is the same as that in the IASP91 Earth model. Synthetic tests indicate that a 1% bias in Vp approximately induces variations of H and k by about 0.5 km and 0.0024, respectively (Nair et al., 2006). The bootstrap resampling approach (Efron and Tibshirani, 1986) with 10 iterations was applied to quantify the mean and standard deviation of the optimal crustal parameters for each station.

Several stations are situated in sedimentary basins or on islands (such as station VNAS located on the Taiping Island of the SCS), and the low-velocity sedimentary layer can produce strong reverberations in the resulting RFs (e.g., Fig. 5a). Such reverberations can completely mask the crustal Ps and its multiples phases associated with the Moho, possibly leading to erroneous H and k measurements (Yu et al., 2015). For such stations, we utilized a resonance-removal filter to suppress the sediment-induced reverberations and isolated the Moho phases (Fig. 5b). The filtered RFs were then employed to determine the crustal structure based on an updated $H - k$ stacking procedure (Yu et al., 2015). Among the 29 stations, 4 of them were processed with the reverberation-removal technique (Table 1).

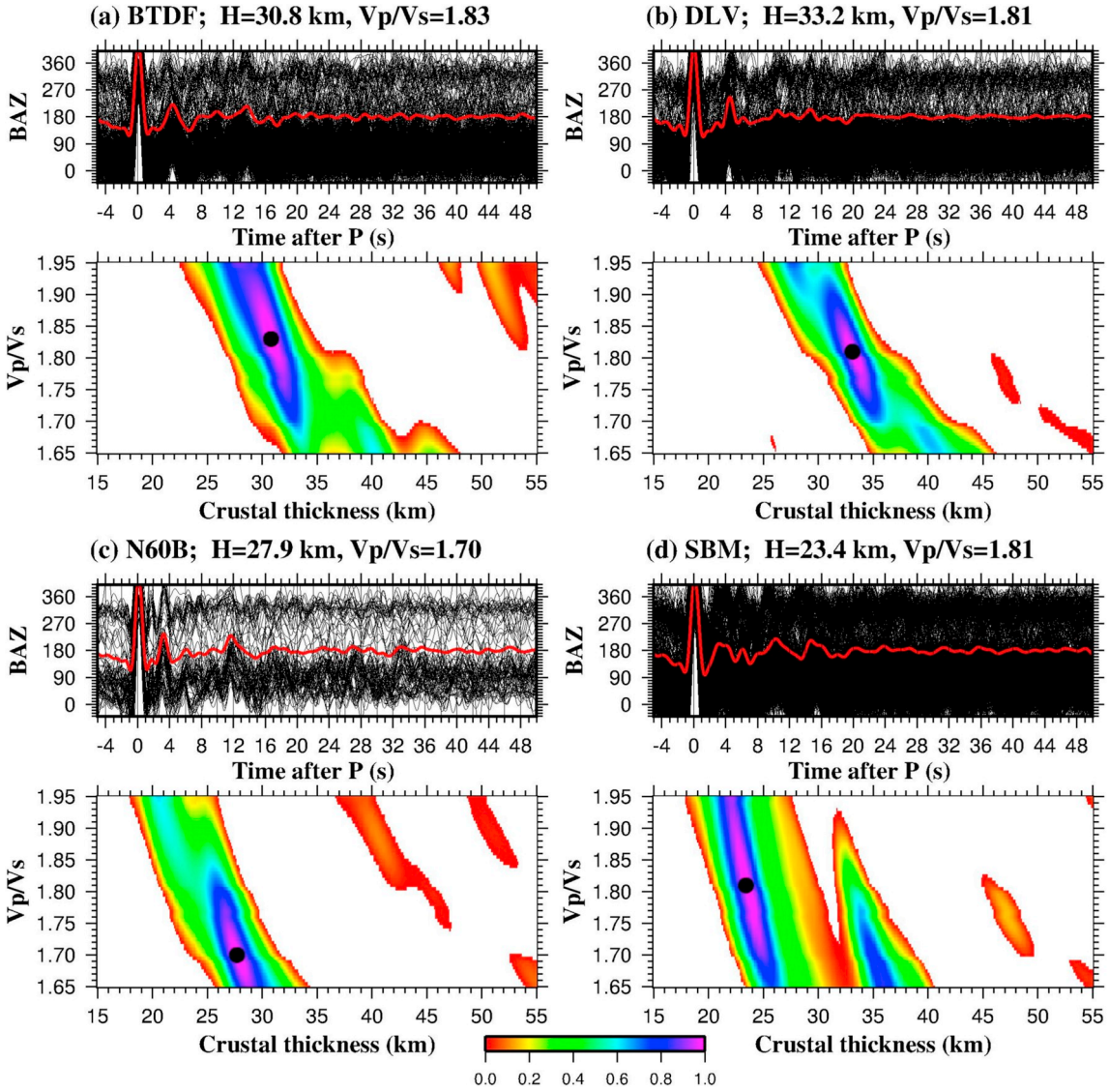

Fig. 4. $H - k$ stacking results from representative stations BTDF (a), DLV (b), N60B (c) and SBM (d), respectively. The upper panel shows a simple time-domain stack (red trace) of all RFs obtained at the station and each individual one (black trace) plotted against back azimuth. The lower panel displays the $H - k$ plot with the black dot corresponding to the maximum stacking amplitude. (For interpretation of the references to colour in this figure legend, the reader is referred to the web version of this article.)

3. Results

After manual checking, 22 of the 29 stations led to reliable crustal thickness and V_P/V_S measurements (Figs. S1–S6) from a total of 17,330 RFs. The number of RFs for each station varies from 18 to 2674 with a simple mean of 788 (Table 1). The resulting H and k measurements show significant spatial heterogeneity (Fig. 6): H ranges from 22.8 km to 39.1 km with a mean value of 28.6 ± 3.7 km, and k changes from 1.68 to 2.12 with an average of 1.81 ± 0.11 (Fig. 6 and Table 1). Relative to the global averages of 34 km and 1.78 for continental crust (Christensen, 1996; Zandt and Ammon, 1995), on average the study area shows thinner H and higher k values. Previous results from additional 5 stations (Latiff and Khalil, 2019; Yu et al., 2017b) in the Indochina Peninsula and Malay Peninsula are also added in Fig. 6 to enhance the spatial coverage of the $H - k$ stacking measurements.

3.1. Borneo Island

Well-defined crustal thickness and V_P/V_S measurements were obtained from three stations on the Borneo Island, which display a contrasting feature between its NE and NW regions. H and k values are similar for stations KSM (24.8, 1.85) and SBM (23.4, 1.81) situated in the Sarawak area of NW Borneo. Such a crustal thickness is in agreement with that obtained from gravity inversion reporting a Moho depth of about 25 km (Khan et al., 2017). In comparison, station KKM in the Sabah region of NE Borneo is underlain by a much thicker crust (39.1 km) and smaller k value (1.71, Fig. 6 and Table 1).

3.2. Indochina Peninsula

Station DLV is situated at the southern tip of the Indochina Peninsula where extensive volcanic rocks are exposed (Fig. 6). The crustal parameters are determined to be 33.2 ± 0.1 km and 1.81 ± 0.00 for H and k, respectively, which are consistent with observations from Yu et al., 2017b.

3.3. Malay Peninsula

The Malay Peninsula contains 7 stations whose H and k are determined to range from 26.2 km to 33.3 km with a mean value of

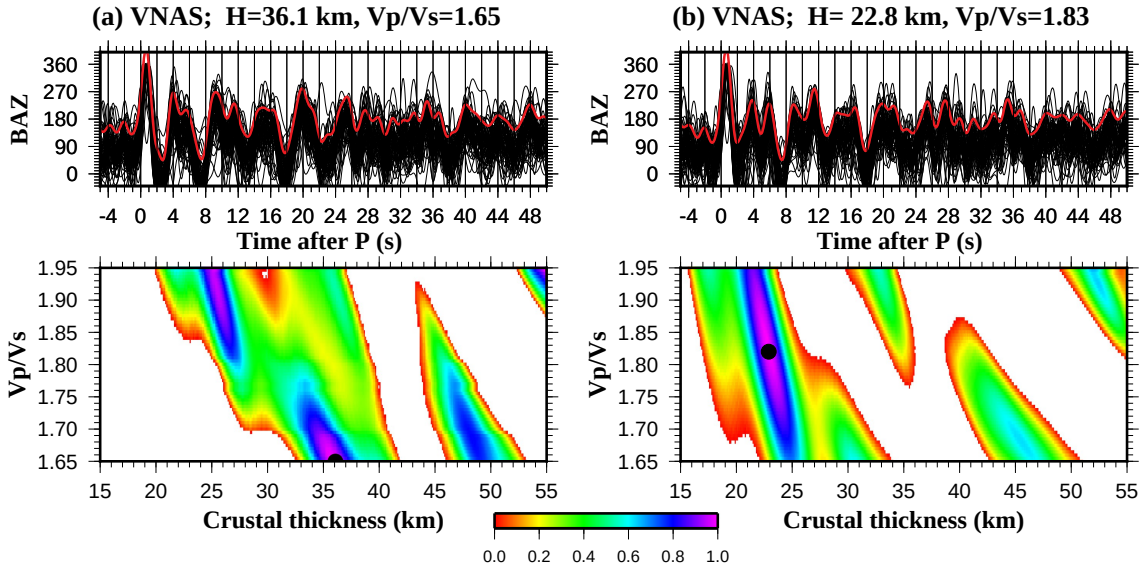

Fig. 5. Same as Fig. 4 but for station VNAS before (a) and after (b) applying the reverberation-removal technique (Yu et al., 2015).

29.7 ± 2.5 km and from 1.68 to 1.83 with an average of 1.76 ± 0.06, respectively. Most of the observed H values are consistent with those from previous studies (Kieling et al., 2011; Latiff and Khalil, 2019; Macpherson et al., 2013; Yu et al., 2017b), but significant discrepancies are revealed in the k ratios (Table 1). Kieling et al. (2011) observed k values of 1.80 and 1.84 at stations KOM and KUM, respectively, which are much higher than the corresponding results of 1.71 and 1.77 from this study. Similarly, higher k values were obtained at stations SKLT (1.83) and SRIT (1.77) based on joint inversion of RF and surface wave dispersion (Latiff and Khalil, 2019) compared with our observations of 1.69 and 1.68, respectively. In addition, k values at stations BTDF and SURA were determined to be 1.74 and 1.72 (Latiff and Khalil, 2019), respectively, which are much smaller than our observations of 1.83 and 1.81.

Table 1
Observations of crustal thicknesses (H) and V_P/V_S (k) values for the 22 stations.

Station	Latitude	Longitude	H (km)	H^* (km)	k	k^*	N. of RFs
A30S	1.171	99.395	26.3 ± 0.3		2.01 ± 0.03		39
BTDF	1.361	103.773	30.8 ± 0.2	32.0[b]	1.83 ± 0.01	1.74[b]	727
				29.5 ± 0.0[c]		1.86 ± 0.00[c]	
DLV	11.952	108.481	33.2 ± 0.1	34.4 ± 0.0[d]	1.81 ± 0.00	1.80 ± 0.00[d]	798
F70S	1.471	99.044	29.6 ± 0.2		2.12 ± 0.02		26
IPM	4.479	101.025	28.4 ± 0.1	24.0–32.0[b]	1.80 ± 0.00	1.77[b]	2179
				24.0[a]			
KKM	6.044	116.215	39.1 ± 0.1		1.71 ± 0.00		981
KOM	1.792	103.847	33.3 ± 0.0	35.0[a]	1.71 ± 0.00	1.80[a]	2030
				34.0[b]		1.75[b]	
KSM	1.473	110.308	24.8 ± 0.0		1.85 ± 0.00		2129
KUM	5.290	100.649	31.4 ± 0.0	33.0[a]	1.77 ± 0.00	1.84[a]	2079
				30.0[b]		1.73[b]	
N20S	1.465	99.468	30.9 ± 0.3		1.86 ± 0.03		44
N40S	1.551	99.695	27.5 ± 0.1		1.78 ± 0.01		141
N50S	1.626	99.743	27.5 ± 0.2		1.73 ± 0.01		102
N60B	1.635	99.883	27.9 ± 0.2		1.70 ± 0.01		95
PSI	2.694	98.924	25.1 ± 0.1	21.0[e]	1.73 ± 0.00	1.72[e]	2674
SBM	2.453	112.214	23.4 ± 0.0		1.81 ± 0.00		2024
SKLT	7.176	100.616	26.2 ± 0.0	26.0[b]	1.69 ± 0.00	1.83[b]	659
SRIT	8.595	99.602	30.8 ± 0.0	28.0[b]	1.68 ± 0.00	1.77[b]	347
				31.7 ± 0.2[d]		1.68 ± 0.01[d]	
SURA	9.166	99.629	27.3 ± 0.5	28.0[b]	1.81 ± 0.03	1.72[b]	96
				27.1 ± 0.3[d]		1.91 ± 0.02[d]	
Results after the removal of sedimentary effects							
A60B	1.387	99.211	29.4 ± 0.4		1.98 ± 0.03		20
L60S	1.145	99.762	26.8 ± 0.5		1.82 ± 0.02		60
N30R	1.493	99.596	26.1 ± 0.3		1.90 ± 0.02		18
VNAS	10.377	114.365	22.8 ± 0.2		1.83 ± 0.01		62

* RF results from previous studies.
[a] Results from Kieling et al. (2011).
[b] Results from Latiff and Khalil (2019).
[c] Results from Macpherson et al. (2013).
[d] Results from Yu et al., 2017b.
[e] Results from Sakaguchi et al. (2006).

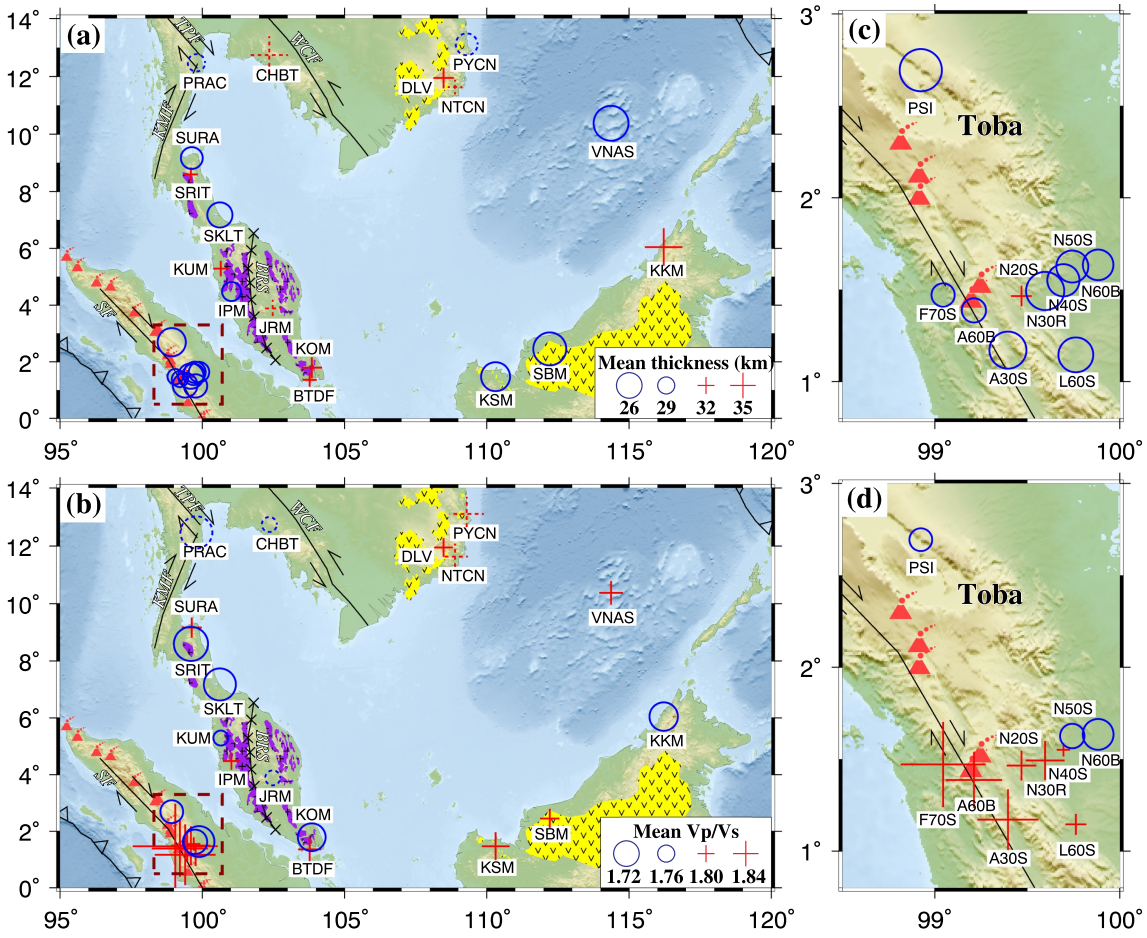

Fig. 6. Resulting crustal thickness and V_P/V_S ratios plotted on topographic map. (c) and (d) show results of areas highlighted by the dark-red dashed rectangle in (a) and (b), respectively. Blue circles and red pluses indicate smaller and larger values, respectively (see legend for detail). Dashed circles and pluses represent crustal measurements from previous studies (Latiff and Khalil, 2019; Yu et al., 2017b). (For interpretation of the references to colour in this figure legend, the reader is referred to the web version of this article.)

3.4. South China Sea

Station VNAS is located on the Taiping Island belonging to the Nansha block at the southern margin of the SCS basin where a low-velocity sedimentary layer exists. After applying the reverberation-removal technique (Yu et al., 2015), we were able to determine the crustal parameters at station VNAS (Fig. 5b). The resulting H and k are 22.8 ± 0.2 km and 1.83 ± 0.01, respectively. Previous crustal thickness studies around the Taiping Island dominantly utilize multi-channel seismic data, and the Moho depth is estimated to be about 24 km (e.g., Qiu et al., 2011; Chang et al., 2017; Yu et al., 2017c), which is comparable to results from this study.

3.5. Sumatra Island

For the 10 stations located on the Sumatra Island (Fig. 6), the resulting H measurements range from 25.1 to 30.9 km with a mean value of 27.7 ± 1.8 km. The thickest crust of 30.9 km is found at station N20S. The k measurements show a systematic increase towards the Toba Caldera and the Sumatra fault, from 1.70 to 2.12 with a higher–than-normal average of 1.86 ± 0.14. An earlier RF study (Sakaguchi et al., 2006) also reveals a widespread distribution of high k values in the vicinity of the Toba Caldera.

4. Discussion

The resulting crustal thickness and k measurements, although sparsely distributed, provide important information on crustal composition and possible modification associated with slab subductions and the evolution of marginal seas. The spatial variation of the resulting H and k values may indicate that the central Sunda plate is not as rigid as previously thought and its crust may have been partially deformed (Hall and Morley, 2004). The existence of compositional variations is supported by the low cross-correlation coefficient of 0.37 between the observed crustal thickness and the corresponding altitude (Fig. 7a). Laboratory and seismic experiments indicate that the k values are closely related to crustal compositions and vary from 1.63 to 2.08 with a mean value of 1.78 (Christensen, 1996; Zandt and Ammon, 1995). Holbrook et al. (1992) conclude that felsic rocks are characterized as possessing k lower than 1.76, intermediate rocks have k values ranging from 1.76 to 1.81 and that for mafic rocks are above 1.81. Based on the above criteria, the overall crustal compositions for different tectonic domains can be generally speculated by referring to the resulting k parameter. In addition, partial melting and fluid content can dramatically increase the k ratios of crustal rocks (Watanabe, 1993).

4.1. Magmatic activities driven by the Indo-Australian subduction

Both the Indochina Peninsula and the Sumatra Island are situated closely to the oblique Indo-Australian subduction zones where magmatic activities are pervasively present (Fitch, 1972; Metcalfe, 2013). The addition of magmatic compositions in the crust can directly change the overall crustal properties, which can be deciphered by the observed crustal H and k. Based on our observations and previous crustal $H - k$

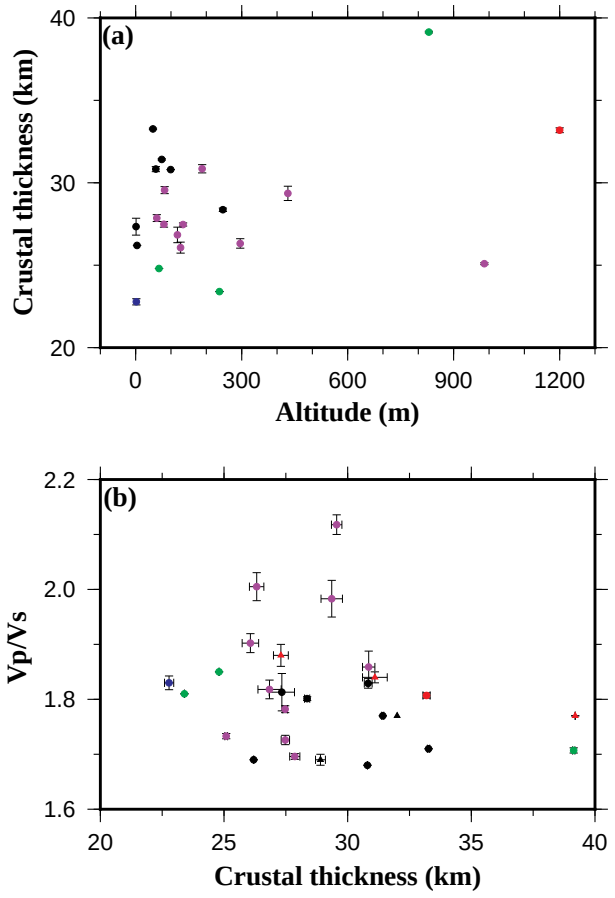

Fig. 7. Plots of crustal thickness against its corresponding altitude (a) and V_P/V_S ratio (b). Colors of dots indicate results belonging to each sub-region: Borneo (green), Sumatra (purple), the Indochina Peninsula (red), the Malay Peninsula (black) and the South China Sea (blue). (For interpretation of the references to colour in this figure legend, the reader is referred to the web version of this article.)

measurements (Yu et al., 2017b), the southern tip of the Indochina Peninsula may be characterized by a mafic bulk composition or crustal partial melting as indicated by the high (> 1.81) k observations, which is consistent with distributions (Fig. 6) of pervasive basaltic magmatism (Hoang and Flower, 1998). These widespread Cenozoic volcanisms are attributable to mantle upwelling triggered by the sinking of the broken-off Indian slab segments (Yu et al., 2017a).

Sumatra is sitting directly above the subducting oceanic Indo-Australian slab, which currently promotes the development of a chain of volcanoes and exerts significant impact on the crustal structure of the overlying plate (Fitch, 1972). The overwhelming and systematic high k ratios observed at Sumatra denote serious modifications of the crust and display an increasing trend towards the Sumatra fault or the Toba Caldera (Fig. 6d) where several large explosive eruptions have occurred in the recent geological past (Koulakov et al., 2016). Partial melting underneath the Toba due to active volcanism has been proposed to interpret the observed high k values (Kieling et al., 2011; Sakaguchi et al., 2006). A regional tomography study focusing on the Toba Caldera reveals a complex multilevel plumbing system underneath and finds that large amounts of overheated volatiles originating in the subducting slab ascend through the crust and promote the formation of melting reservoir for the super-eruptions (Koulakov et al., 2016). Most of our observations at Sumatra approximately fall into the impact zone of a slab window originated due to slab tear (Koulakov et al., 2016; Kong et al., 2020), which could offer additional heating for the observed crustal modification. In addition, the Sumatra fault may act as an efficient pathway for the fluid-rich or volatile-rich partially molten magmas to migrate upward, which may explain the extremely high k values observed close to the fault. Thus, our observations indicate that the compositions and degree of partial melting of the crust at Sumatra have been significantly altered by the complex magmatic activities associated with the Indo-Australian subduction processes.

4.2. Effects of Cenozoic rifting and thermal anomaly on the crustal properties of the Malay Peninsula

The continental core of the Malay Peninsula is believed to be the result of crustal thickening with a long history of early and late Mesozoic collisions associated with both island arc and post-collision magmatism, and appears to be relatively undeformed after the Triassic Indosinian orogeny (e.g., Metcalfe, 2013; Sautter et al., 2017). Pervasive magmatic rocks are found at the Malay Peninsula and have been divided into eastern and western belts approximately along the Bentong-Raub Suture (Fig. 1). The western belt is dominantly composed of S-Type group of granitoids generated by crustal thickening in the period of late Triassic to earliest Jurassic (Metcalfe, 2013). In comparison, the eastern belt has U-Pb zircon ages of Permian to Middle Triassic and comprises mainly I-type subduction-related granitoids consisting of monzogranite, granodiorite, gabbro, diorite and tonalite (Searle et al., 2012). These granitoids have been proposed to result from subduction of the Palaeo-Tethys beneath Indochina-East Malaya (Metcalfe, 2013; Sone and Metcalfe, 2008).

Our observations beneath the Malay Peninsula are inconsistent with the northwards decreasing pattern of crustal thickness revealed from a recently joint inversion of surface wave dispersion and RF (Latiff and Khalil, 2019). Instead, a spatially heterogeneous pattern of crustal structure is revealed. Crust beneath the East Malay block (32.0 ± 1.3 km) is generally at least 3 km thicker than that beneath the Sibumasu terrane (28.8 ± 2.2 km, Fig. 6), which could be attributed to the joint effects of Cenozoic rifting and thermal anomaly. Structural synthesis and correlation of basins across the Malay Peninsula (Sautter et al., 2017) suggest that rifting activities started to develop in the entire region by the end of the Eocene (35–30 Ma) and were followed by a thermal anomaly in the Oligocene/Earliest Miocene (30–20 Ma). Laboratory experiments (Yang et al., 1997) indicate that the S-type granitoid is more sensitive to the temperature variations and becomes easier to melt relative to the I-type granitoid. The crustal thinning revealed at the Sibumasu terrane relative to the East Malay block is possibly associated with the existence of dominantly S-type granitoid. The thinned crust is weakened by the Oligocene thermal anomaly and further promotes crustal stretching driven by the continuous Eocene rifting event. In addition, it has been proposed that the crustal thickness at the Sibumasu terrane (43 km) is about 13 km thicker than that of the East Malay block by the end of the late Triassic (Ghani et al., 2013; Metcalfe, 2000), suggesting that the crust at the Sibumasu terrane has been thinned by roughly 30%.

The absence of widespread high (> 1.81) k ratios possibly indicates that partial melting or fluid content associated with the currently active Indo-Australian subduction may not strongly influence the crustal structure beneath the Malay Peninsula. Instead, most parts of the Malay Peninsula are determined to have crustal compositions of generally felsic to intermediate rocks. One exception is station BTDF situated at the southeastern corner of the East Malay block with a k value of 1.83, which is possibly resulted from the intrusion of mafic dykes. Analysis of geochronological data indicates that basaltic dykes are dominantly found at the East Malay block and 98% of them were determined to possess an age of 79 ± 2 Ma (Ghani et al., 2013).

4.3. Crustal modifications associated with the evolution of the South China Sea

It has been proposed that slab-pull of the proto-SCS (e.g., Hall, 2002; Clift et al., 2008) existing between South China margin and

Borneo works as one of the mechanisms to drive the seafloor spreading of the present SCS between Oligocene and Middle Miocene (Taylor and Hayes, 1983). The continuously southward subduction of the Proto-SCS could bring extensive volcanisms and promote the development of an accretionary prism at Borneo (Clift et al., 2008). Geological studies (Khan et al., 2017) propose that lower crust melting and underplating during Oligocene-Miocene occurred due to subducting young oceanic crust under felsic continental crust of the Sarawak area and give rise to volcanic activities (Hutchison, 1996), a hypothesis that is consistent with the observed high k values (Fig. 6). These magmatic activities can significantly modify the crustal compositions like what is occurring beneath Sumatra. Crustal thickness at the Sarawak region is calculated to be 24.1 km, which is almost the same as what revealed from gravity inversion with a value of about 25 km and indicates a passive margin setting (Khan et al., 2017). In contrast, the Sabah area at NE Borneo possesses a much thicker crust (39.1 km) with a felsic composition derived from a k value of 1.71 (Fig. 6 and Table 1), which possibly implies an accretionary margin. Since the caseation of the Proto-SCS subduction in the Early Miocene, the thinned passive margin of South China (the Nansha block) collided with NE Borneo, which initiated the Sabah orogeny and further induced crustal thickening observed at station KKM (Hall, 2002; Hall et al., 2008).

Station VNAS is situated at the Taiping Island belonging to the Nansha block, which is believed to be separated from the South China margin and moved southwards to the present position due to the spreading of the SCS basin (Hall, 1996, 2002). Continental origin of the crust at the Taiping Island is supported by the observed thicker crust (22.8 km) compared with the globally average 7 km thickness of the oceanic crust and is also consistent with what revealed from active seismic surveys that the Moho depth is determined to be about 24 km (e.g., Qiu et al., 2011; Chang et al., 2017; Yu et al., 2017c). The continental crust of the Nansha block becomes thinner with the extension of the SCS. The prominent high k ratio (1.83) at station VNAS indicates a mafic composition of the crust, which is incompatible with the conclusion of normal crust revealed from a seismic reflection study (Qiu et al., 2011) and is possibly attributed to magmatic activities associated with the evolution of the SCS. Middle Miocene to Pleistocene sills, dykes, and plutonic materials have been observed near the Nansha area (Schlüter et al., 1996). Inversion of multi-channel seismic and gravity data offshore north of Taiping Island further reveal volcanic basement structure at lower crust, which is interpreted as a result of volcanism originated from a small-scale mantle convection or the afterwards hyper extension in the distal margins (Chang et al., 2017). Systematic analysis of seismic reflection data covering the whole SCS proposed that igneous emplacement mostly occurred after the spreading cessation and the widespread post-spreading magmatic activities are possibly triggered by thermal cracking, extension and decompression melting in response to the subsidence of the cooling SCS oceanic lithosphere (Song et al., 2017). Thus, more research works are needed to clarify the cause of the widespread post-spreading volcanisms. Nevertheless, the RF results from station VNAS provide independent evidence to confirm the continental origin of the Nansha block and reveal the significant magmatic modification of the crustal composition associated with the evolution of the SCS.

5. Conclusions

Our observations reveal significant spatial heterogeneities in crustal structures beneath the central Sunda plate. The Sumatra Island is characterized by widespread high V_P/V_S values (> 1.81), which may be attributed to fluid-rich or volatile-rich melting from the Indo-Australian subduction. Magmatic activities are also revealed at NW Borneo and the southern margin of the SCS where thinned crust (about 23 km) and high V_P/V_S values are observed, which also offer independent evidence on the fact that the post-spreading volcanism of the SCS has significantly modified the crustal composition of the Nansha block. Crustal thickening is revealed at NE Borneo, probably due to the underthrust of the Nansha block since the cessation of the southward Proto-SCS subduction. The Malay Peninsula is generally characterized as possessing felsic-to-intermediate crustal compositions while crustal thinning is revealed beneath the Sibumasu terrane whose crust is at least 3 km thinner than that of the East Malay block, which is possibly induced by the joint effects of Cenozoic rifting and thermal anomaly.

CRediT authorship contribution statement

Jia Gao: Investigation, Methodology, Writing - original draft. **Youqiang Yu**: Supervision, Conceptualization, Writing - original draft, Writing - review & editing. **Wenkai Song**: Methodology, Software. **Stephen S. Gao**: Writing - review & editing. **Kelly H. Liu**: Writing - review & editing.

Declaration of competing interest

The authors declare that they have no known competing financial interests or personal relationships that could have appeared to influence the work reported in this paper.

Acknowledgments

Data used in this study are archived at, and were provided by, the Incorporated Research Institutions for Seismology Data Management Center (https://ds.iris.edu/ds/nodes/dmc/; Last accessed: January 2019) under seismic networks of MS, MY, PS, RM, TM, TW and ZB. The facilities of IRIS Data Services (https://www.iris.edu/) were used for access to waveforms. Comments from editor Vernon Cormier and two anonymous reviewers greatly improved the manuscript. This work was funded by the National Program on Global Change and Air-Sea Interaction (grant GASIGEOGE-05) and the National Natural Science Foundation of China (grant 41606043).

Appendix A. H-k stacking plots for 22 stations

Supplementary figures to this article can be found online at https://doi.org/10.1016/j.pepi.2020.106539.

References

Ammon, C.J., 1991. The isolation of receiver effects from teleseismic P waveforms. Bull. Seismol. Soc. Am. 81 (6), 2504–2510.
Bird, P., 2003. An updated digital model of plate boundaries. Geochem. Geophys. Geosyst. 4, 1027. https://doi.org/10.1029/2001GC000252.
Briais, A., Patriat, P., Tapponnier, P., 1993. Updated interpretation of magnetic anomalies and seafloor spreading stages in the South China Sea: implications for the tertiary tectonics of Southeast Asia. J. Geophys. Res. 98 (B4), 6299–6328. https://doi.org/10.1029/92JB02280.
Chang, J.H., Hsieh, H.H., Mirza, A., Chang, S.P., Hsu, H.H., Liu, C.S., Su, C.C., Chiu, S.D., Ma, Y.F., Chiu, Y., Hung, H.T., Lin, Y.C., Chiu, C.H., 2017. Crustal structure north of the Taiping Island (Itu Aba Island), southern margin of the South China Sea. J. Asian Earth Sci. 142, 119–133. https://doi.org/10.1016/j.jseaes.2016.08.005.
Christensen, N.I., 1996. Poisson's ratio and crustal seismology. J. Geophys. Res. 101 (B2), 3139–3156. https://doi.org/10.1029/95JB03446.
Clift, P., Lee, G.H., Anh Duc, N., Barckhausen, U., Van Long, H., Zhen, S., 2008. Seismic reflection evidence for a dangerous grounds miniplate: no extrusion origin for the South China Sea. Tectonics 27 (3), TC3008. https://doi.org/10.1029/2007TC002216.
Efron, B., Tibshirani, R., 1986. Bootstrap methods for standard errors, confidence intervals, and other measures of statistical accuracy. Stat. Sci. 1 (1), 54–75. https://doi.org/10.1214/ss/1177013815.
Fitch, T.J., 1972. Plate convergence, transcurrent faults, and internal deformation adjacent to southeast Asia and the western Pacific. J. Geophys. Res. 77 (23), 4432–4460. https://doi.org/10.1029/JB077i023p04432.
Flower, M.F.J., Tamaki, K., Hoang, N., 1998. Mantle extrusion: A model for dispersed volcanism and DUPAL-like asthenosphere in East Asia and the western Pacific. In: Flower, M.F.J., Chung, S.L., Lo, C.H. (Eds.), Mantle Dynamics and Plate Interactions in East Asia, Geodynamics. American Geophysical Union, Washington, DC, pp. 67–88.
Ghani, A.A., Lo, C.H., Chung, S.L., 2013. Basaltic dykes of the Eastern Belt of Peninsular

Malaysia: the effects of the difference in crustal thickness of Sibumasu and Indochina. J. Asian Earth Sci. 77, 127–139. https://doi.org/10.1016/j.jseaes.2013.08.004.
Hall, R., 1996. Reconstructing Cenozoic SE Asia. Geol. Soc. Lond., Spec. Publ. 106 (1), 153–184. https://doi.org/10.1144/GSL.SP.1996.106.01.11.
Hall, R., 2002. Cenozoic geological and plate tectonic evolution of SE Asia and the SW Pacific: computer-based reconstructions, model and animations. J. Asian Earth Sci. 20 (4), 353–431. https://doi.org/10.1016/S1367-9120(01)00069-4.
Hall, R., Morley, C.K., 2004. Sundaland basins. In: Clift, P., Wang, W., Kuhnt, H. (Eds.), Continent-Ocean Interactions Within the East Asian Marginal Seas Geophysical Monograph. 149. American Geophysical Union, Washington, DC, pp. 55–85.
Hall, R., van Hattum, M.W., Spakman, W., 2008. Impact of India–Asia collision on SE Asia: the record in Borneo. Tectonophysics 451 (1–4), 366–389. https://doi.org/10.1016/j.tecto.2007.11.058.
Hoang, N., Flower, M., 1998. Petrogenesis of Cenozoic basalts from Vietnam: implication for origins of a 'diffuse igneous province'. J. Petrol. 39 (3), 369–395. https://doi.org/10.1093/petroj/39.3.369.
Holbrook, W.S., Mooney, W.D., Christensen, N.I., 1992. The seismic velocity structure of the deep continental crust. In: Fountain, D.M., Arculus, R., Kay, R.W. (Eds.), Continental Lower Crust. Elsevier, New York, pp. 21–43.
Hutchison, C.S., 1996. The 'Rajang accretionary prism' and 'Lupar Line' problem of Borneo. Geol. Soc. Lond., Spec. Publ. 106 (1), 247–261. https://doi.org/10.1144/GSL.SP.1996.106.01.16.
Khan, A.A., Abdullah, W.H., Hassan, M.H., Iskandar, K., 2017. Tectonics and sedimentation of SW Sarawak basin, Malaysia, NW Borneo. J. Geol. Soc. India 89 (2), 197–208. https://doi.org/10.1007/s12594-017-0584-0.
Kieling, K., Roessler, D., Krueger, F., 2011. Receiver function study in northern Sumatra and the Malaysian peninsula. J. Seismol. 15 (2), 235–259. https://doi.org/10.1007/s10950-010-9222-7.
Kong, F., Gao, S.S., Liu, K.H., Zhang, J., Li, J., 2020. Seismic anisotropy and mantle flow in the Sumatra subduction zone constrained by shear wave splitting and receiver function analyses. Geochem. Geophys. Geosyst. 21 (2), e2019GC008766. https://doi.org/10.1029/2019GC008766.
Koulakov, I., Kasatkina, E., Shapiro, N.M., Jaupart, C., Vasilevsky, A., El Khrepy, S., Al-Arifi, N., Smirnov, S., 2016. The feeder system of the Toba supervolcano from the slab to the shallow reservoir. Nat. Commun. 7 (1), 12228. https://doi.org/10.1038/ncomms12228.
Latiff, A.H.A., Khalil, A.E., 2019. Crustal thickness and velocity structure of Malay Peninsula inferred from joint inversion of receiver functions and surface waves dispersion. J. Asian Earth Sci. 169, 105–116. https://doi.org/10.1016/j.jseaes.2018.08.011.
Liu, K.H., Gao, S.S., 2010. Spatial variations of crustal characteristics beneath the Hoggar swell, Algeria, revealed by systematic analyses of receiver functions from a single seismic station. Geochem. Geophys. Geosyst. 11 (8), Q08011. https://doi.org/10.1029/2010GC003091.
Macpherson, K.A., Hidayat, D., Feng, L., Goh, S.H., 2013. Crustal thickness and velocity structure beneath Singapore's seismic network. J. Asian Earth Sci. 64, 245–255. https://doi.org/10.1016/j.jseaes.2012.12.027.
McCaffrey, R., 2009. The tectonic framework of the Sumatran subduction zone. Annu. Rev. Earth Planet. Sci. 37, 345–366. https://doi.org/10.1146/annurev.earth.031208.100212.
Metcalfe, I., 2000. The Bentong–Raub suture zone. J. Asian Earth Sci. 18 (6), 691–712. https://doi.org/10.1016/S1367-9120(00)00043-2.
Metcalfe, I., 2002. Permian tectonic framework and palaeogeography of SE Asia. J. Asian Earth Sci. 20 (6), 551–566. https://doi.org/10.1016/S1367-9120(02)00022-6.
Metcalfe, I., 2011. Tectonic framework and Phanerozoic evolution of Sundaland. Gondwana Res. 19 (1), 3–21. https://doi.org/10.1016/j.gr.2010.02.016.
Metcalfe, I., 2013. Tectonic evolution of the Malay Peninsula. J. Asian Earth Sci. 76, 195–213. https://doi.org/10.1016/j.jseaes.2012.12.011.
Nair, S.K., Gao, S.S., Liu, K.H., Silver, P.G., 2006. Southern African crustal evolution and composition: constraints from receiver function studies. J. Geophys. Res. 111 (B2), B02304. https://doi.org/10.1029/2005JB003802.
Qiu, X., Zhao, M., Ao, W., Hao, T., You, Q., Ruan, A., Li, J., 2011. OBS survey and crustal structure of the Southwest Sub-basin and Nansha Block, South China Sea. Chin. J. Geophys. 54 (12), 1009–1021. https://doi.org/10.1002/cjg2.1680.
Rangin, C., Le Pichon, X., Mazzotti, S., Pubellier, M., Chamot-Rooke, N., Aurelio, M., Walpersdorf, A., Quebral, R., 1999. Plate convergence measured by GPS across the Sundaland/Philippine Sea plate deformed boundary: the Philippines and eastern Indonesia. Geophys. J. Int. 139 (2), 296–316. https://doi.org/10.1046/j.1365-246x.1999.00969.x.
Replumaz, A., Kárason, H., van der Hilst, R.D., Besse, J., Tapponnier, P., 2004. 4-D evolution of SE Asia's mantle from geological reconstructions and seismic tomography. Earth Planet. Sci. Lett. 221 (1–4), 103–115. https://doi.org/10.1016/S0012-821X(04)00070-6.
Replumaz, A., Tapponnier, P., 2003. Reconstruction of the deformed collision zone Between India and Asia by backward motion of lithospheric blocks. J. Geophys. Res. 108(B6), 2285. doi:10.1029/2001JB000661.
Sakaguchi, K., Gilbert, H., Zandt, G., 2006. Converted wave imaging of the Toba Caldera, Indonesia. Geophys. Res. Lett. 33 (20), L20305. https://doi.org/10.1029/2006GL027397.
Sautter, B., Pubellier, M., Jousselin, P., Dattilo, P., Ierdraon, Y., Choong, C.M., Menier, D., 2017. Late Paleogene rifting along the Malay Peninsula thickened crust. Tectonophysics 710, 205–224. https://doi.org/10.1016/j.tecto.2016.11.035.
Schlüter, H.U., Hinz, K., Block, M., 1996. Tectono-stratigraphic terranes and detachment faulting of the South China Sea and Sulu Sea. Mar. Geol. 130 (1–2), 39–78. https://doi.org/10.1016/0025-3227(95)00137-9.
Searle, M.P., Whitehouse, M.J., Robb, L.J., Ghani, A.A., Hutchison, C.S., Sone, M., Ng, S.W.P., Roselee, M.H., Chung, S.L., Oliver, G.J.H., 2012. Tectonic evolution of the Sibumasu–Indochina terrane collision zone in Thailand and Malaysia: constraints from new U–Pb zircon chronology of SE Asian tin granitoids. J. Geol. Soc. 169 (4), 489–500. https://doi.org/10.1144/0016-76492011-107.
Sieh, K., Natawidjaja, D., 2000. Neotectonics of the Sumatran fault, Indonesia. J. Geophys. Res. 105 (B12), 28295–28326. https://doi.org/10.1029/2000JB900120.
Sone, M., Metcalfe, I., 2008. Parallel Tethyan sutures in mainland Southeast Asia: new insights for Palaeo-Tethys closure and implications for the Indosinian orogeny. Compt. Rendus Geosci. 340 (2–3), 166–179. https://doi.org/10.1016/j.crte.2007.09.008.
Song, X., Li, C.F., Yao, Y., Shi, H., 2017. Magmatism in the evolution of the South China Sea: geophysical characterization. Mar. Geol. 394, 4–15. https://doi.org/10.1016/j.margeo.2017.07.021.
Sun, W., 2016. Initiation and evolution of the South China Sea: an overview. Acta Geochimica 35 (3), 215–225. https://doi.org/10.1007/s11631-016-0110-x.
Tapponnier, P., Peltzer, G., Le Dain, A.Y., Armijo, R., Cobbold, P., 1982. Propagating extrusion tectonics in Asia: new insights from simple experiments with plasticine. Geology 10 (12), 611–616. https://doi.org/10.1130/0091-7613(1982)10<611:PETIAN>2.0.CO;2.
Taylor, B., Hayes, D.E., 1983. Origin and history of the South China Sea basin. In: Hayes, D.E. (Ed.), The Tectonic and Geologic Evolution of Southeast Asian Seas and Islands (Part 2), Geophysical Monograph Series. 27. American Geophysical Union, Washington, D. C, pp. 23–56. https://doi.org/10.1029/GM027p0023.
Watanabe, T., 1993. Effects of water and melt on seismic velocities and their application to characterization of seismic reflectors. Geophys. Res. Lett. 20 (24), 2933–2936. https://doi.org/10.1029/93GL03170.
Yang, S.F., Chen, H.L., Jiang, J.S., Zhu, G.Q., Xie, H.S., Hou, W., Zhang, Y.M., Xu, H.G., 1997. Properties of wave velocity for two types of granitoids at high pressure and temperature and their geological meaning. Sci. China. Ser. D Earth Sci. 40 (5), 470–476. https://doi.org/10.1007/BF02877611.
Yu, Y., Gao, S.S., Liu, K.H., Yang, T., Xue, M., Le, K.P., 2017a. Mantle transition zone discontinuities beneath the Indochina Peninsula: implications for slab subduction and mantle upwelling. Geophys. Res. Lett. 44 (14), 7159–7167. https://doi.org/10.1002/2017GL073528.
Yu, Y., Hung, T.D., Yang, T., Xue, M., Liu, K.H., Gao, S.S., 2017b. Lateral variations of crustal structure beneath the Indochina Peninsula. Tectonophysics 712, 193–199. https://doi.org/10.1016/j.tecto.2017.05.023.
Yu, Z., Li, J., Ding, W., Zhang, J., Ruan, A., Niu, X., 2017c. Crustal structure of the Southwest Subbasin, South China Sea, from wide-angle seismic tomography and seismic reflection imaging. Mar. Geophys. Res. 38 (1–2), 85–104. https://doi.org/10.1007/s11001-016-9284-1.
Yu, Y., Song, J., Liu, K.H., Gao, S.S., 2015. Determining crustal structure beneath seismic stations overlying a low-velocity sedimentary layer using receiver functions. J. Geophys. Res. 120 (5), 3208–3218. https://doi.org/10.1002/2014JB011610.
Zandt, G., Ammon, C.J., 1995. Continental crust composition constrained by measurements of crustal Poisson's ratio. Nature 374 (6518), 152–154. https://doi.org/10.1038/374152a0.
Zhu, L., Kanamori, H., 2000. Moho depth variation in southern California from teleseismic receiver functions. J. Geophys. Res. 105 (B2), 2969–2980. https://doi.org/10.1029/1999JB900322.